ENHANCEMENT OF WIRELESS POWER TRANSMISSION INTO BIOLOGICAL TISSUES USING A HIGH SURFACE IMPEDANCE GROUND PLANE

Sung Il Park[*]

Department of Electrical Engineering, Stanford University, CA 94305, USA

Abstract—The system which enhances wireless power transmission efficiency for bio-medical applications has been proposed in this report. The system that operates at giga-hertz ranges is based on an inductive coupling between a transmitter coil and a receiver coil. A magnetic current source was modeled to a magnetic dipole with magnetic dipole moment m. To increase wireless power transmission efficiency, a high surface impedance ground plane was used and reflection from the ground plane is responsible for constructive interference. For this system, a theoretical study has been performed in this report by solving Sommerfeld integrals. Compared with the result of a system without a ground plane, the system with a high surface impedance ground plane showed enhancement of received power at a given transmitted power.

1. INTRODUCTION

Medical devices implanted into the human body such as pacemakers, physiological monitoring devices, pain relief devices, drug infusion pumps, cochlear hearing implants, and artificial hearts have become popular in biomedical applications [1–3]. The continued scaling of electronic components is accelerating the development of biomedical microsystems, and the development of new microelectromechanical systems technologies is rapidly changing the landscape of the medical and electronics industry. These devices allow monitoring or the communication of the internal vital signals to the external system. In these devices, power supplies are made by contactless power transmission. Wireless power transmission is a very useful and reliable method in cases where interconnecting wires are not convenient,

feasible or possible. In biomedical applications such as a power source for a pacemaker, and a micro-robot implanted into the human body, this contactless power transmission is desirable because there is a potential risk of battery failure in a pacemaker and the wireless method can solve the issue. For this reason, contactless power transfer has recently gained scientific interest and many studies pertaining to the advanced technology relating to it have been aggressively investigated [4–7]. These systems are powered by an inductive coupling method, and an inductively coupled wireless power transfer system consists of two coils which are referred to as primary, corresponding to a transmitter, and secondary associated with a receiver coil. In these systems, power transfer efficiency depends on the size of the coil, the distance between coils, and the environment surrounding coils. Efficiency is very limited, especially depending on the spacing between a primary and secondary coil, because the coupling becomes negligible when the distance is far from the near-field region. Recently, the system based on a magnetic resonance coupling has been demonstrated [8, 9]. This non-radiative power transfer system showed much higher transfer efficiency than that of an inductively coupling power transfer system in the broader region. Since the system is made with a magnetic resonant coupling, the efficiency is less restricted in the environment surrounding the coils.

For bio-medical applications, frequency ranging mega-hertz has been extensively used to deliver power via the wireless method. This was based on the false idea that electromagnetic waves significantly attenuate as frequency increases when propagating biological tissues such as muscle and skin. However, it has been shown that biological tissues such as skin, muscle, and bone are closer to dielectrics than a conductor at the low giga-hertz frequency ranges as in [10]. As shown in [10], maximum power transmission efficiency at the low giga-hertz frequency ranges was achieved. An optimized transmitter structure with the maximum power transfer efficiency has been proposed [11]. One powerful advantage of using high frequency is to reduce the size of the coil, and the reduction of size enables the researcher to implant a micro-robot into the body by supplying power via the wireless method. For this reason, at mega-hertz ranges the miniaturization of the system is limited. Overall, the efficiency of an inductively coupling wireless power transfer system at giga-hertz frequency ranges is lower than that of a magnetic resonant coupling system whereas the former outweighs the latter in terms of the size of a system. This report investigates the potential of implementing an inductively coupling wireless power transfer system at giga-hertz frequency ranges based on a high surface impedance plane, and analyzes the system by solving Sommerfeld

equations with the goal of providing insight on how to enhance power transfer efficiency.

This report is organized as follows: Section 2 introduces the background of how the efficiency is enhanced. Section 3 proposes the system with a high surface impedance ground plane and analyzes the system by solving Sommerfeld equations, and field distribution of each system are plotted. In Section 4, heating issues in biological tissues caused by absorption of electromagnetic waves was considered based on the guideline. Section 5 summarizes the system.

2. BACKGROUND

The most common form of wireless power transmission is performed by direct induction coupling, which is governed by Faraday's law, between coils [12]. This magnetic induction is a simple model of near-field electromagnetic interaction. The near-field differs from the far-field in which the field acts as electromagnetic radiation. Although the boundary between the two regions is indecisively distinguished, it depends on the dominant wavelength (λ) emitted by the source and near-field region is generally defined as within a quarter wavelength. The far-field region is not considered in this report.

Figure 1 shows the background of how the system enhances power transmission [12]. When an electric dipole source is located vertically on the perfect electric conductor plane, the ground plane reflects incident waves coming from a source and results in constructive interference with waves in the other direction. Finally, the power transmission is enhanced as shown in Figure 1(a). On the other hand, fields are balanced out or interfered with destructively because the 180 degree phase shift occurs on the perfect conductor plane when an electric source is located horizontally on the perfect electric conductor plane. According to the duality of the electromagnetic wave, when a magnetic dipole source is placed vertically on the perfect magnetic conductor plane, the ground plane reflects incident waves emitting from the dipole source as shown in Figure 1(b). The perfect electric plane has infinity conductance, whereas the perfect magnetic plane has conductivity of zero, or infinity resistance. The total field above the ground plane is equal to the sum of the direct and reflected components, which indicates that reflected waves are interfered with incident waves constructively or destructively according to the direction of a source.

The concept of a high surface impedance plane having infinity surface impedance is not new. Corrugated surface structures and mushroom shaped structures showed very high surface
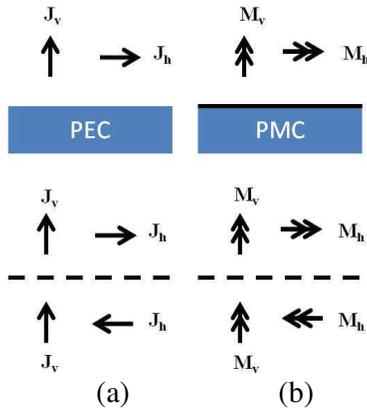
Figure 1. Illustration of the image theory. (a) Fields on a perfect electric conductor (PEC) ground plane and their images. (b) Fields on a perfect magnetic conductor (PMC) ground plane and their images. The single arrow indicates an electric element and the double one corresponds to a magnetic element. The direction of the arrow identifies the polarity. J_h (M_h) is a horizontal electric (magnetic) source. J_v (M_v) is a vertical electric (magnetic) source.
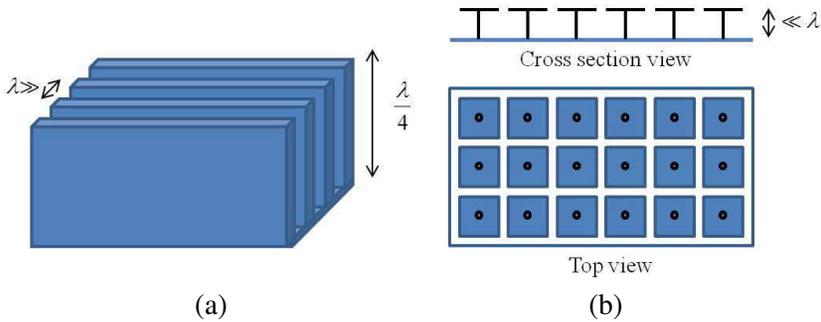
Figure 2. A high surface impedance ground plane. (a) Corrugated surface. (b) Mushroom shaped structure.

impedance [13, 14]. The principle of how high surface impedance at the surface is achieved is very simple. Assume that 'teeth' are very thin compared with wavelength and there are many slots per wavelength. As shown in Figure 2(a), the tangential component of an incident electric field wave is zero at the bottom of a corrugated surface, which indicates zero resistance, according to the boundary

condition. When its depth is equal to a quarter wavelength, however, zero conductance is achieved at the top of the surface because the 180 degree phase shift occurs on the perfect electric conductor plane, and the phase shift is balanced out after traveling a half wavelength. This corresponds to high surface impedance. Similarly, Figure 2(b) showed a mushroom shaped structure which is characterized by high surface impedance. The plane consists of an array of metal protrusions on a flat conductor plane and the period of the surface texture is much smaller than the wavelength. This indicates that the characteristic of high surface impedance is implemented by lumped circuit elements such as a capacitor and an inductor. Each protrusion can be modeled to a parallel resonant circuit which can permit finite normal component fields and infinity tangential component fields, which result in high surface impedance (E_x/H_y) [14].

To analyze the wave propagation through biological tissues, an appropriate model should be used. The spectrum of biological tissue such as muscle, skin, fat, and bone can be emulated via the multiple Cole-Cole relaxation dielectric model [15, 16]. At the low giga-hertz ranges the model can be approximated by [15],

$$k \approx \omega\sqrt{\mu_0\varepsilon_0\varepsilon_{r0}} + i\frac{\omega}{2}\sqrt{\frac{\mu_0\varepsilon_0}{\varepsilon_{r0}}}\left[\frac{\delta}{\omega\varepsilon_0} + \omega\tau(\varepsilon_{r0} - \varepsilon_\infty)\right] \qquad (1)$$

where δ is conductivity, τ is the relaxation time constant, ε_{r0} is the static relative permittivity, and ε_∞ is the relative permittivity at frequencies where $\omega\tau \gg 1$. For muscle, δ is 0.2, τ is 7.2 pico-second, ε_{r0} is 50, and ε_∞ is 4 at 2 GHz.

The Sommerfeld equation was solved analytically with this information. For the rest of the sections, the scattered field was ignored because the scattered field associated with the induced current density is negligible compared with the incident field caused by the transmitted magnetic current density [10].

3. ANALYSIS

A general inhomogeneous profile such as dispersive media can be expressed by layers of piecewise constant regions. Since the rule of thumb is to approximate the layers such that they are much thinner than the wavelength of the wave in the medium [17], the plane wave analysis which doesn't take into account a source region is not appropriate [10, 18]. Thus, a source region was considered in this report. The human body can be emulated by a planarly layered medium as shown in Figure 3(a) although the model which incorporates biological tissues in an idealized cylindrical limb can
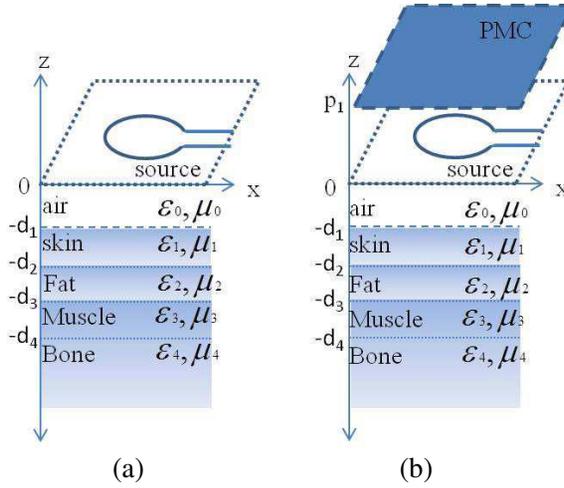
Figure 3. Dielectric models of human body and an air-muscle half space model. $\varepsilon_{0,1,...}$ and $\mu_{0,1,...}$ are the permittivity and permeability respectively in each layer.

describe characteristics of each dielectric medium more precisely [19]. The tangential component of electromagnetic waves in each medium can be written as [17],

$$e_{it} = A_i \left[e^{-ik_{iz}z} + \tilde{R}_{i,i+1} e^{ik_{iz}z + 2ik_{iz}d_i} \right] \quad (2)$$

A_i & $\tilde{R}_{i,i+1}$ can be recursively obtained by the boundary condition such as the continuity of the tangential field at each interface [17]. This model, shown in Figure 3(a), is expected to require intensive computational work. Although the wave propagation and electromagnetic fields distribution in the human body can be described in more detail for the model shown in Figure 3(a), the air-muscle half space model was used to lessen computation work load and simplify the analysis. This approximation doesn't affect the result and conclusion addressed in this report.

Electromagnetic wave propagating through inhomogeneous media such as biological tissues can be obtained by Sommerfeld integrals [20]. Sommerfeld solved the problem of a vertical electric or magnetic dipole on top of a half space using Hertzian potentials. Many results can be achieved without intensive computational work. In addition, closed-form solutions in terms of spectral integrals enable not only their asymptotic approximations, but provide more physical insight into the problems. For a vertical magnetic dipole (VMD) source as shown in

Figure 4(a), electromagnetic fields are given by [17],

$$H_{1z} = -\frac{m}{8\pi\omega\mu} \int_{-\infty}^{\infty} dk_\rho \frac{k_\rho^3}{k_{1z}} H_0^{(1)}(k_\rho\rho) \times \left[e^{-ik_{1z}z} + R_{TE}e^{ik_{1z}z+2ik_{1z}d_1} \right]$$
$$-d_1 < z < p_1 \quad (3)$$

$$H_{2z} = -\frac{m}{8\pi\omega\mu} \int_{-\infty}^{\infty} dk_\rho \frac{k_\rho^3}{k_{1z}} H_0^{(1)}(k_\rho\rho) T_{TE1} e^{-ik_{2z}(z+d_1)+ik_{1z}d_1}$$
$$z < -d_1 \quad (4)$$

where $H_0^{(1)}$ is the first kind of zero-order Hankel function, m is magnetic moment, $k_{1,2z} = \sqrt{k_{1,2}^2 - k_\rho^2}$, $R_{TE} = \frac{k_{1z}-k_{2z}}{k_{1z}+k_{2z}}$, and $T_{TE1} = \frac{2k_{1z}}{k_{1z}+k_{2z}}$.

In the case of the system using a PMC plane in Figure 4(b), electromagnetic fields are as follows.

$$H_{1z} = -\frac{m}{8\pi\omega\mu} \int_{-\infty}^{\infty} dk_\rho \frac{k_\rho^3}{k_{1z}} H_0^{(1)}(k_\rho\rho)$$
$$\times \left[e^{|ik_{1z}z|} + A_{TE}e^{-ik_{1z}z} + B_{TE}e^{ik_{1z}z} \right] \quad -d_1 < z < p_1 \quad (5)$$

$$H_{2z} = -\frac{m}{8\pi\omega\mu} \int_{-\infty}^{\infty} dk_\rho \frac{k_\rho^3}{k_{1z}} H_0^{(1)}(k_\rho\rho) T_{TE2} e^{-ik_{2z}(z+d_1)+ik_{1z}d_1} \quad z < -d_1 \quad (6)$$

where $H_0^{(1)}$ is the first kind of zero-order Hankel function, m is magnetic moment, $A_{TE} = \frac{R_{TE}+e^{-2ik_{1z}d_1}}{-R_{TE}+e^{-2ik_{1z}(p_1+d_1)}}$, $B_{TE} = \frac{R_{TE}+R_{TE}e^{-2ik_{1z}p_1}}{-R_{TE}+e^{-2ik_{1z}(p_1+d_1)}}$,
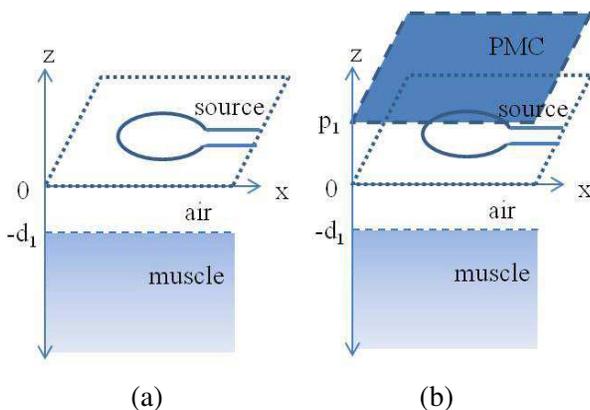
Figure 4. An air-muscle half space model. (a) Reference. (b) The system with a high surface impedance ground plane.

$T_{TE2} = \frac{T_{TE1}(1+e^{-2ik_{1z}p_1})}{-R_{TE}+e^{-2ik_{1z}(p_1+d_1)}}$, and $k_{1,2z}$ and R_{TE} are the same as the above case.

The total magnetic flux incident on the receiver coil or dipole is $\mu_0 H_{2z}(z) \cdot \hat{n} A_r$, where $\hat{n}$ is the unit vector perpendicular to the surface of the receiver coil. The rate of change of total magnetic flux passing through the coil produces the induced emf in the coil according to Faraday's law of induction. Assuming that the receiver consists of a coil and a load resistor, Z_L, received power can be expressed as,

$$P_R = \frac{|i\omega\mu H_{2z}(z) \cdot \hat{n} A_r|^2}{2R_L} \tag{7}$$

Received power distributions of each system in muscle are plotted in Figures 5(a) and (b). For better comparison, the same legend in each plot was used. Since wavelength (frequency of 2 giga-hertz) in muscle corresponds to 2 cm, the grid size of 1 mm, which is less than $\frac{1}{10\lambda}$, was chosen to minimize the error that will be caused by the resolution. Assuming that the receiver system is facing in z direction, which maximizes the induced emf. In both cases, electromagnetic fields decrease monotonically as the source is away from the receiver coil. This is consistent with the characteristics of electromagnetic waves emitted from a point source because waves propagate isotropically.

The system with a PMC plane shows better performance in terms of the power transmission efficiency. As shown in Figure 5(c), at a given transmitted power 5 dB higher signal is received at the receiver. Figure 5(d) compared the received power of the system based on a PMC plane with that of the system without any ground plane in terms of p_1 which corresponds to a distance between a source and a PMC plane. As a source approaches the ground plane, the reflection become dominant and in turn the received power is enhanced. Overall, a PMC plane promotes the coupling in a broader region. The enhancement is due to the reflection from the high surface impedance ground plane and a function of the distance between a source and a ground plane.

For (3) $\sim$ (6), the source is a point magnetic dipole with magnetic moment $m = iA$ where A is the area of the coil. When a magnetic current source distribution, $M_1(r)$, such as a uniform source or a phased array source is used, one can solve the electric field and the magnetic field as follows [17],

$$E(r) = -\int_{-\infty}^{\infty}\int_{-\infty}^{\infty} dr' G_e\left(r - r'\right) M\left(r'\right) \tag{8}$$

$$H(r) = i\omega\varepsilon \int_{-\infty}^{\infty}\int_{-\infty}^{\infty} dr' G_h\left(r - r'\right) M\left(r'\right) \tag{9}$$
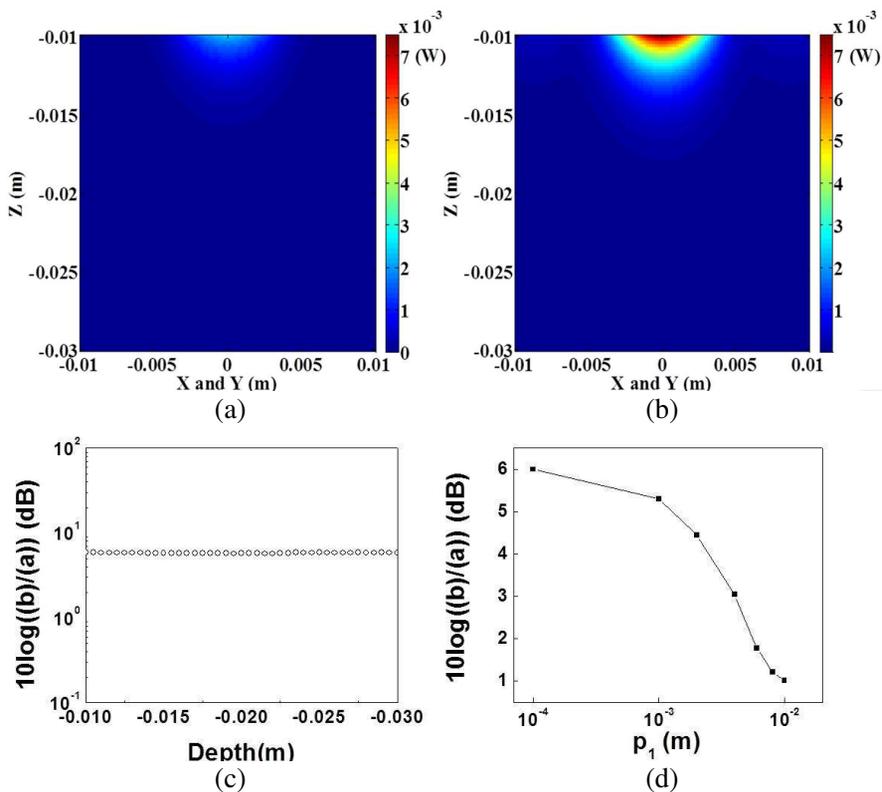
Figure 5. Received power distributions of each case. (a) The system without a PMC plane and (b) the system with a PMC plane. (c) Power gain $10 \cdot \log$ (power of the system with a PMC plane/power of the reference system). (d) Power gain at the point ($x = 0$, $y = 0$, and $d_1 = -0.01$ m) in terms of p_1 which corresponds to a distance between a source and a PMC plane. For (a), (b), and (c), $\lambda = 0.02$ m in muscle and $p_1 = 0.003$ m. d_1 is the distance between a source and the air-muscle interface. Load resistance was 1 ohm, and the area of the receiver coil as 4 mm^2.

where G_e and G_h are the dyadic Green's functions. Dyadic Green's functions, which relates a vector field to a vector current source, of a vector wave equation is the solution of the vector wave equation for a point source or dipole. For some electromagnetic problems, more succinct forms of solutions can be made by the use of Green's functions, and this symbolic compact form of solution can give us more insight into these problems. Although most problems can be

solved without using it, the simplicity they can offer makes their use attractive. Once Green's functions is found, the solution associated with a general source, $M(r)$, can be obtained by the principle of linear superposition as written in (8) and (9). Equations (8) and (9) can also be expressed,

$$E(r) = -\int_{-\infty}^{\infty}\int_{-\infty}^{\infty} dk_\rho \tilde{G}_e(k_\rho, z)\tilde{M}(k_\rho, z) \qquad (10)$$

$$H(r) = i\omega\varepsilon \int_{-\infty}^{\infty}\int_{-\infty}^{\infty} dk_\rho \tilde{G}_h(k_\rho, z)\tilde{M}(k_\rho, z) \qquad (11)$$

where $\tilde{G}_e$ and $\tilde{G}_h$ are the dyadic Green's functions in the spectral domain. Field components in (3) $\sim$ (6) can be seen as Dyadic Green's functions because those are the solution of the vector equation for dipole, and one can solve (8) and (9) by finding $\tilde{G}_e$ and $\tilde{G}_h$, substituting $\tilde{M}(k\rho, z)$ into (10) and (11), and taking inverse Fourier transform.

For a phased array source (N by N) as shown in Figure 6, magnetic current source distribution, $M(r)$, is given as,

$$M(r) = \sum_{i=1}^{N}\sum_{j=1}^{N} a_{ij}\delta(x - x_{ij}, y - y_{ij}), \qquad (12)$$

where a_{ij} is a coefficient and x_{ij} and y_{ij} are the location of each point source in a phased array.
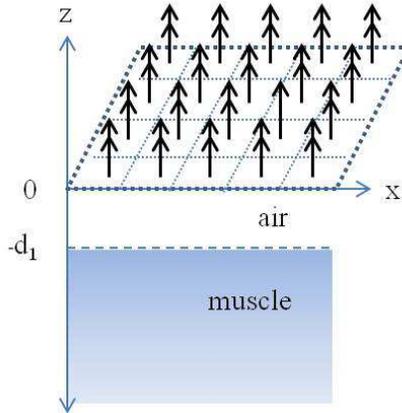
Figure 6. Illustration of N by N a phased array source. Double arrows indicate a magnetic dipole source with magnetic moment. A focal point is a function of the number of sources and a coefficient of each sources.

Double arrows indicate each vertical magnetic dipole source and a phased array source is designed to focus electromagnetic fields emitted from sources on the focal point whereas electromagnetic fields from a point source propagate isotropically, and a point source itself is not feasible for focusing as shown in Figures 4(a) and (b). Coefficients, a_{ij}, correspond to the phase of each vertical magnetic dipole with respect to the reference magnetic dipole, and x_{ij} and y_{ij} can be a quarter, half, or one wavelength such that the emitted field from each source contributes to constructive or destructive interference.

Figure 7 shows the received power distribution of each system. In both cases, fields are concentrated at the focal point (1 cm below the air-muscle interface), which indicates that the power can be delivered in more efficient ways. The system with a PMC plane showed higher received power than the system without a PMC plane. This is consistent with the result shown in Figure 5 and indicates that the system is independent of source types. Hence, this can be applied to any source type such as a point source, uniform source, or a phased array source. The enhancement is also due to the reflection from the high surface impedance ground plane and a function of the distance between a source and a ground plane.
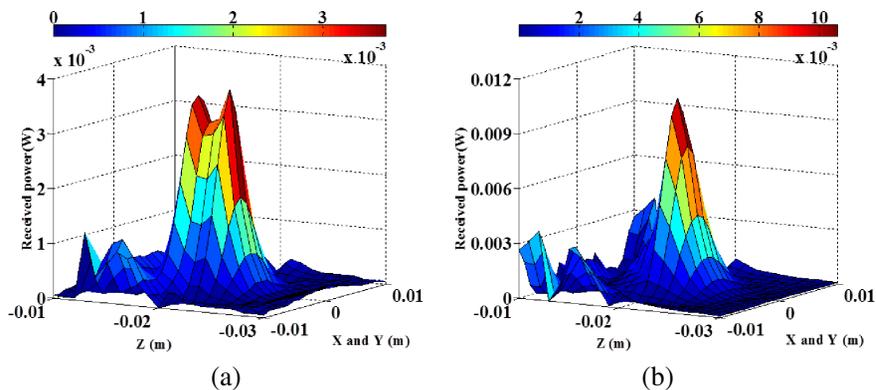
Figure 7. Received power distribution of each system. (a) The system without any ground plane and (b) the system with a PMC plane. The magnetic current source was designed to be a focal point of 1 cm below the air-muscle interface. The distance between a source and the air-muscle interface, d_1, was -0.01 m, $\lambda = 0.02$ m in muscle, and $p_1 = 0.001$ m. Load resistance was 1 ohm, and the area of the receiver coil as $4\,\text{mm}^2$.

4. DISCUSSION

Guidelines of safety levels with respect to human exposure to radio frequency electromagnetic fields are described in IEEE Standard C95.1-2005 [21]. These recommendations are expressed in terms of maximum permission exposure (MPEs) and specific absorption ratio (SAR) values. The SAR can be expressed in terms of $\delta \frac{E(r)}{\rho}^2$ where δ is the tissue conductivity (S/m), ρ is the tissue density (kg/m^3) and $E(r)$ is the root mean square (rms) electric field strength in tissue (V/m). For power transfer via the inductive coupling method, the heating of the tissue caused by radio frequency electromagnetic fields is a primary safety concern. According to the guideline, the tissue absorption must be kept to less than $1.6\,\mathrm{mW}$ in $1\,\mathrm{cm}^3$, and in general the tissue temperature rise should not exceed 1–2°C to avoid a damage caused by overheating in sensitive areas such as the brain [22]. It has been found that sub-millimeter to millimeter watt of power transmission can be safely made for a millimeter sized coil with a separation of a few centimeter at giga hertz frequency range [10], and millimeter watt of power transmission was considered in this work. In addition, tissue absorption is less because a magnetic current source, where magnetic near field is much higher than their electric near field, was considered.

In this study, it was assumed that the high surface impedance ground plane is lossless. When the distance between the ground plane and a source is close to zero, maximum enhancement of $6\,\mathrm{dB}$ was achieved. In reality, the ground plane is not perfect and there exists loss on the plane. Therefore, to maximize enhancement the scattering parameter, S_{11}, should be minimized as possible when designing the ground plane.

5. CONCLUSION

An inductively coupling wireless power transmitter based on a high surface impedance ground plane that operates at giga-hertz frequency range has been proposed. The ground plane reflects electromagnetic waves emitted from a source, and the reflected waves are in the same phase, as are the incident waves. This makes for constructive interference, and in turn the power transfer efficiency is enhanced. To analyze the system, Sommerfeld integrals have been solved. The perfect magnetic conductor or a high surface impedance ground plane can be implemented by a corrugate surface structure or a mushroom shaped ground plane. The system produces higher efficiency than the structure without a PMC plane and is independent of source types such as a point source, uniform source, or a phased array source.

REFERENCES

1. Akin, T., K. Najafi, and R. M. Bradley, "A wireless implantable multichannel digital neural recording system for a micromachined sieve electrode," *IEEE Journal of Solid-State Circuits*, Vol. 33, 109–118, 1998.

2. Liu, W., K. Vichienchom, M. Clements, S. C. DeMarco, C. Hughes, E. McGucken, M. S. Humayun, E. DeJuan, J. D. Weiland, and R. Greenberf, "A neuro-stimulus chip with telemetry unit for retinal prosthetic device," *IEEE Journal of Solid-State Circuits*, Vol. 35, 1487–1497, 2000.

3. Sauer, C., M. Stanacevic, G. Cauwenberghs, and J. N. Thakor, "Power harvesting and telemetry in CMOS for implanted devices," *IEEE Trans. Circuit Syst. I*, Vol. 52, 2605–2613, 2005.

4. Baker, M. W. and R. Sarpeshkar, "Feedback analysis and design of RF power links for low-power bionic systems," *IEEE Trans. Biomed. Circuits Syst.*, Vol. 1, 28–38, 2007.

5. Harrison, R., "Designing efficient inductive power links for implantable devices," *Proc. 2007 IEEE Intl. Symposium on Circuits and Systems (ISCAS 2007)*, 2080–2083, New Orleans, 2007.

6. Neihart, N. M. and R. Harrison, "Micropower circuits for bidirectional wireless telemetry in neural recording applications," *IEEE Trans. Biomed. Eng.*, Vol. 52, 1950–1959, 2005.

7. Smith, S., T. Tang, J. Terry, J. T. M. Stevenson, B. W. Flynn, H. M. Reekie, A. F. Murray, A. M. Gundlach, D. Renshaw, B. Dhillon, A. Ohtori, Y. Inoue, and A. J. Walton, "Development of a miniaturised drug delivery system with wireless power transfer and communication," *IET Nanobiotechnology*, Vol. 1, 80–86, 2007.

8. Kurs, A., A. Karalis, R. Moffatt, J. D. Joannopoulos, P. Fisher, and M. Soljacic, "Wireless power transfer via strongly coupled magnetic resonances," *Science*, Vol. 317, 83–86, 2007.

9. Ramrakhyani, A. K., S. Mirabbasi, and M. Chiao, "Design and optimization of resonance-based efficient wireless power delivery systems for biomedical implants," *IEEE Trans. Biomed. Circuits Syst.*, Vol. 5, 48–63, 2011.

10. Poon, A. S. Y., S. O'Driscoll, and T. H. Meng, "Optimal frequency for wireless power transmission into dispersive tissue," *IEEE Trans. Antennas Propagat.*, Vol. 58, 739–1749, 2010.

11. Kim, S. and A. S. Y. Poon, "Wireless power transfer into miniature implants: Transmitter optimization," *IEEE Trans. Antennas Propagat.*, Vol. 60, 4838–4845, 2012.

12. Jackson, J. D., *Classical Electrodynamics*, John Wiley & Sons, 1999.

13. Cutler, C. C., "Genesis of the corrugated electromagnetic surface," *IEEE Int. Antennas Propagat. Symp. Dig.*, Vol. 32, 1456–1459, 1944.

14. Sievenpiper, D. F., "High-impedance electromagnetic surfaces," Ph.D. Dissertation, Department of Electrical Engineering, University of California, Los Angeles, 1999.

15. Gabriel, S., R. W. Lau, and C. Gabriel, "The dielectric properties of biological tissues: III. Parametric models for the dielectric spectrum of tissues," *Phys. Med. Biol.*, Vol. 41, 2271–2293, 1996.

16. Vorst, A. V., *RF/Microwave Interaction with Biological Tissues*, Wiley-IEEE Press, 2006.

17. Chew, W. C., *Waves and Fields in Inhomogeneous Media*, Wiley-IEEE Press, 1995.

18. Andersen, J. B., "Theoretical limitations on radiation into muscle tissue," *Int. J. Hyperthermia*, Vol. 1, 45–55, 1985.

19. Lowery, M. M., N. S. Stoykov, A. Taflove, and T. A. Kuiken, "A multiple-layer finite-element model of the surface EMG signal," *IEEE Trans. Biomed. Eng.*, Vol. 49, 446–454, 2002.

20. Sommerfeld, A., *Partial Differential Equations in Physics*, Academic Press, 1949.

21. "IEEE standard for safety levels with respect to human exposure to radio frequency electromagnetic fields, 3 kHz to 300 GHz," IEEE Standard C95.1-2005, 2006.

22. Wise, K. D., A. M. Sodagar, Y. Yao, M. N. Gulari, G. E. Perlin, and K. Najafi, "Microelectrodes, microelectronics, and implantable neural microsystems," *Proc. IEEE*, Vol. 96, 1184–1202, 2008.